

Simulated and experimental studies of a multi-band symmetric metamaterial absorber with polarization independence for radar applications

Hema O. Ali, Asaad M. Al-Hindawi, Yadgar I. Abdulkarim, Ekasit Nugoolcharoenlap, Tossapol Tippo, Fatih Özkan Alkurt, Olcay Altıntaş, and Muharrem Karaaslan

Citation: Chin. Phys. B, 2022, 31 (**5**): 058401. DOI: 10.1088/1674-1056/ac2b1c
Journal homepage: http://cpb.iphy.ac.cn; http://iopscience.iop.org/cpb

What follows is a list of articles you may be interested in

A radar-infrared compatible broadband absorbing surface: Design and analysis

Qing-Tao Yu(余庆陶), Yuan-Song Zeng(曾元松), and Guo-Jia Ma(马国佳)
Chin. Phys. B, 2021, 30 (**7**): 078402. DOI: 10.1088/1674-1056/abea7f

Estimation of sea clutter inherent Doppler spectrum from shipborne S-band radar sea echo

Jin-Peng Zhang(张金鹏), Yu-Shi Zhang(张玉石), Xin-Yu Xu(许心瑜), Qing-Liang Li(李清亮), Jia-Ji Wu(吴家骥)
Chin. Phys. B, 2020, 29 (**6**): 068402. DOI: 10.1088/1674-1056/ab888a

Equivalent electromagnetic parameters for microwave metamaterial absorber using a new symmetry model

Junming Zhang(张峻铭), Donglin He(何东霖), Guowu Wang(王国武), Peng Wang(王鹏), Liang Qiao(乔亮), Tao Wang(王涛), Fashen Li(李发伸)
Chin. Phys. B, 2019, 28 (**5**): 058401. DOI: 10.1088/1674-1056/28/5/058401

Correction of failure in antenna array using matrix pencil technique

S U Khan, M K A Rahim
Chin. Phys. B, 2017, 26 (**6**): 068401. DOI: 10.1088/1674-1056/26/6/068401

Metallic spherical anechoic chamber for antenna pattern measurement

Ali Farahbakhsh, Mohammad Khalaj-Amirhosseini
Chin. Phys. B, 2016, 25 (**8**): 088401. DOI: 10.1088/1674-1056/25/8/088401

Simulated and experimental studies of a multi-band symmetric metamaterial absorber with polarization independence for radar applications

Hema O. Ali[1], Asaad M. Al-Hindawi[1], Yadgar I. Abdulkarim[2,†], Ekasit Nugoolcharoenlap[3], Tossapol Tippo[3], Fatih Özkan Alkurt[4], Olcay Altıntaş[4], and Muharrem Karaaslan[4]

[1] *Department of Communication Engineering, Sulaimani Polytechnic University, Sulaimani* 46001, *Iraq*

[2] *Medical Physics Department, College of Medicals and Applied Science, Charmo University, Chamchamal* 46023, *Sulaimania, Iraq*

[3] *Department of Telecommunication Engineering, Faculty of Engineering, Rajamangala University of Technology Rattanakosin, Phutthamonthon, Nakornprathom* 73170, *Thailand*

[4] *Department of Electrical and Electronics Engineering, Iskenderun Technical University, Hatay* 31100, *Turkey*

(Received 12 May 2021; revised manuscript received 14 September 2021; accepted manuscript online 29 September 2021)

We develop a simple new design for a multi-band metamaterial absorber (MTMA) for radar applications. Computer Simulation Technology (CST) Studio Suite 2018 was used for the numerical analysis and absorption study. The simulated results show four high peaks at 5.6 GHz, 7.6 GHz, 10.98 GHz, and 11.29 GHz corresponding to absorption characteristics of 100%, 100%, 99%, and 99%, respectively. Furthermore, two different structures were designed and compared with the proposed MTMA. The proposed structure remained insensitive for any incident angle and polarization angle from 0° to 60°. Moreover, negative constitutive parameters were retrieved numerically. To support the simulated results, the proposed design was fabricated by using a computer numerical control-based printed circuit board prototyping machine and tested experimentally in a microwave laboratory. The absorption mechanism of the proposed MTMA is presented through the surface current and electric field distributions. The novelties of the proposed structure are a simple and new design, ease of fabrication, low cost, durability, suitability for real-time applications and long-term stability given the fabrication technique and non-destructive measurement method and very high absorption. The proposed structure has potential applications in C and X band frequency ranges.

Keywords: multi-band, metamaterials, absorber, polarization-independent, negative parameters

PACS: 84.40.Xb, 07.57.–c **DOI:** 10.1088/1674-1056/ac2b1c

1. Introduction

The absorption of electromagnetic waves in the microwave region is a crucial issue in applications such as stealth, cloaking, energy harvesting and so on. Materials which have the property of near-perfect signal absorption are required for these fields of application. Metamaterial (MTM) based structures, which have strong electrical and magnetic coupling features, can meet this need for perfect absorption at certain frequency ranges or points. MTMs with a periodic design and unusual electromagnetic properties have been used in many research fields such as sensors,[1–4] energy harvesters,[5–7] antennas,[8–10] cloaking,[11–13] perfect lenses,[14–16] and so on. They have been investigated by researchers for the last two decades and have many advantages such as ease of configuration, ease of production and low cost.

MTM absorbers (MTMAs) have been explored in a wide range of frequency bands in microwave and terahertz regimes.[17–26] Alkurt *et al.* proposed a microwave power imaging method with a MTMA at a frequency of 2.51 GHz.[17] Schottky diodes have been used to harvest energy obtained by the absorber. Bilal *et al.* suggested a wideband perfect MTMA in the 20 GHz–30 GHz frequency range.[18] The absorber structure was specially designed to be E-shaped and can be useful in 5G communications applications. Abdulkarim *et al.* investigated a novel multi-band MTMA with polarization insensitivity and wide incident angle stability at frequencies of 2.75 GHz, 4.3 GHz, and 9.5 GHz.[19] Han *et al.* achieved a novel miniaturized tri-band MTMA in the terahertz frequency regime with angular and polarization stability. The structure provided perfect signal absorption at 0.33 THz, 0.62 THz, and 0.82 THz.[20] Mahmud *et al.* numerically realized a sandwich-type MTMA with a star-shaped resonator. The proposed structure offered 96.77% average absorption for the optical spectrum with wide-angle polarization insensitivity.[21] Zamzam *et al.* examined four models of an MTMA in the terahertz regime. These researchers achieved perfect signal absorption at four different frequency points having a wide angle to the incident wave.[22] Yadgar *et al.* proposed an ultra-thin dual-band perfect MTMA in the terahertz range using a new design of ZnSe substrate.[23] Ghosh *et al.* suggested an ultra-wideband and ultra-thin MTMA with circular split rings for the X band regime.[24] A perfect MTMA for a different polarization-independent based design was reported in Refs. [25–27]. Researchers have also been interested

†Corresponding author. E-mail: Yadgar.abdulkarim@charmouniversity.org

© 2022 Chinese Physical Society and IOP Publishing Ltd

in developing a novel design of a triple-band polarization-independent MTMA for C and X band applications.[28,29] Yueyi and colleagues proposed independent phase modulation for quadruplex polarization channels enabled by chirality-assisted geometric-phase metasurfaces.[30] Other related work on a polarization-engineered no interleaved metasurface for integer and fractional orbital angular momentum multiplexing was carried out by Kuang and colleagues.[31] Ali and Al-Hindawi proposed a design for a broadband thin MTMA that covered the frequency range of Ku and K bands. The proposed structure provided a wide bandwidth with a compatible overall size. The designed absorber consisted of a combination of an octagonal disk and split octagon resonator.[32]

In this paper, a multi-band MTMA is proposed for C and X band applications. The proposed structure can cope with a wide range of incident angles and is polarization-insensitive due to its symmetrical design features. It is numerically designed based on three models. The electric field and surface current distribution of the proposed structure were investigated at the absorption peak frequencies. The MTMA was manufactured from 7×5 unit cells using a printed circuit board prototyping machine. The experimental studies were realized using an Agilent PNA-L vector network analyzer (VNA) with a proper horn antenna covering the C and X band frequency regime. Perfect absorption peaks greater than 99% were observed at four frequency points (5.6 GHz, 7.6 GHz, 10.98 GHz, and 11.29 GHz). The proposed structure is a good candidate for implementation in many areas such as the military, communications and medicine. Generally, such absorbers are used in medical applications including medical imaging, reducing electromagnetic hazards to humans and improving the performance of medical sensors. We believe that our absorber is suitable for some of these applications. In particular, frequency scaling means that the proposed structure can be used in any desired frequency range.

2. Theory of the designed structure and numerical results

In this current work, a new multi-band MTMA is designed and theoretically discussed with regard to use in satellite communications and radar applications. A Computer Simulation Technology (CST) based finite integration technique was used for the design process and to obtain numerical results. The proposed MTMA consists of three basic layers from top to bottom, as follows: the top layer is a copper resonator, the middle layer is a substrate and the bottom layer is a ground plane (see Fig. 1).

The resonator is optimized to obtain high-absorption peaks and consists of a circular shape inside a quadratic and two L shapes; the resonator and ground plane are made of copper and have a thickness of 0.035 mm and conductivity σ of 5.8×10^7 S/m. The dielectric layer (the used substrate) is made from FR4 material with a relative permittivity of 4.4 and loss tangent ($\tan\delta$) of 0.02. The thickness of the substrate was chosen to be 1.6 mm. FR4 substrate is used in our design due its advantages of availability in the market, low price, high mechanical strength and low losses.

The required dimensions, structure and the position of the resonator are determined so as to work in the desired frequency range between 4 GHz and 12 GHz. The designed multi-band MTMA is optimized using a genetic algorithm which is built into a function in the software to control the impedance matching for all operating frequencies. The required dimensions of the designed structure are shown in Table 1.

Table 1. The dimensions required for the multi-band MTMA.

Parameter	W_s	L_s	W	L	b	r_1	r	i	P	N	M	s
Value (mm)	18	18	3.8	9.17	0.27	2	2.6	0.35	0.8	6.3	2.02	0.25

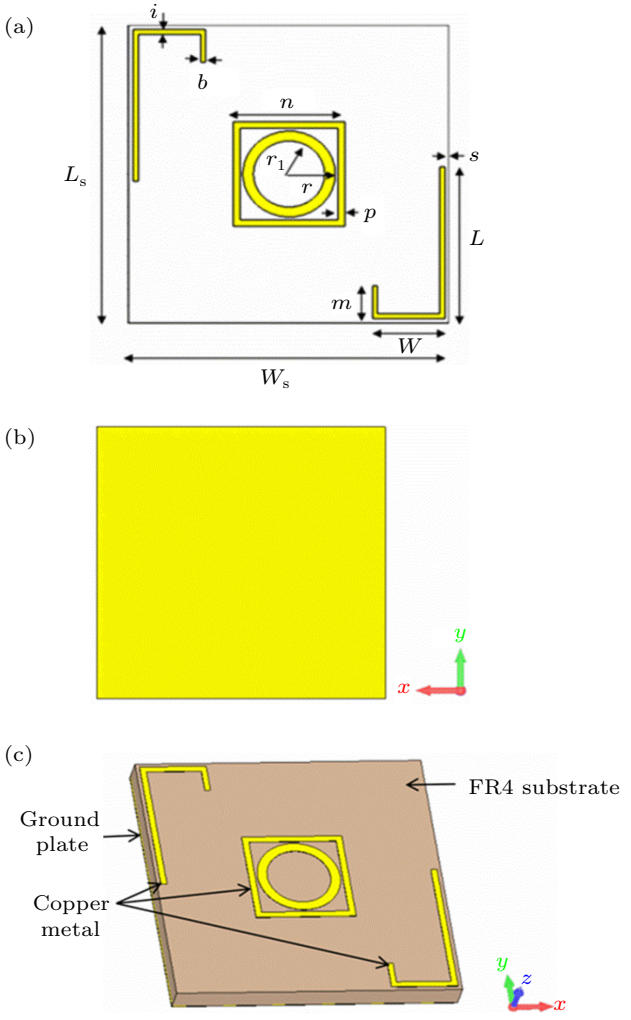


Fig. 1. The designed multi-band MTMA: (a) dimensions and front view, (b) back view and (c) perspective view.

In this work, to obtain perfect absorption the reflection of the designed structure should be minimized and the absorber impedance matched with the free space impedance $Z(\omega) = Z_0$.

For all MTMAs, the effective permeability (μ) and the permittivity (ε) of the medium can be expressed by the equation

$$Z(\omega) = \sqrt{\frac{\mu_0 \mu_r(\omega)}{\varepsilon_0 \varepsilon_r(\omega)}}, \tag{1}$$

where $Z(\omega)$ is the intrinsic impedance.

When $Z(\omega) = Z_0$, the reflection coefficient $\Gamma(\omega)$ will be zero and there is no reflected wave,

$$\Gamma(\omega) = \frac{Z(\omega) - Z_0}{Z(\omega) + Z_0}. \tag{2}$$

The reflection of the proposed structure can be determined by numerical simulation, then the absorption of the multi-band MTMA structure can be found using

$$A(\omega) = 1 - R(\omega) - T(\omega), \tag{3}$$

where the reflection coefficient and transmission coefficient are denoted by $R(\omega) = |S_{11}|^2$ and $T(\omega) = |S_{21}|^2$, respectively. The back of the proposed structure is covered by a copper metal plate and its thickness is much greater than the skin depth, therefore there is no transmission through the structure ($T(\omega) = 0$) and Eq. (3) is reduced to the following form:

$$A(\omega) = 1 - R(\omega). \tag{4}$$

Figure 2(a) shows the simulated results of the reflection and absorption for the proposed structure in the frequency range 4 GHz–12 GHz. There are several boundary conditions within the CST software such as periodic, perfect electric conduction, perfect magnetic conduction, open add space and unit cell. In this work, X and Y axes were set to be in the unit cell direction while the Z-axis set to be open add space for compatibility with the experimental setup. The reflection coefficient of the designed structure was obtained and is illustrated by the red curve in Fig. 2(a). The reflection coefficient has four peaks, with the maximum peak reaching -30 dB and the minimum peak being approximately -13 dB. By using Eq. (4), the absorptivity of the proposed structure can be determined, as shown by the blue curve. The absorber has four high-absorption peaks at 5.6 GHz, 7.6 GHz, 10.98 GHz, and 11.29 GHz, respectively corresponding to absorptivities of 100%, 100%, 99%, and 99%. Each of the center frequencies has a band according to the -10 dB reflection criterion. Therefore, the absorber has three operating frequency bands including 5.5 GHz–5.7 GHz, 7.5 GHz–7.7 GHz, and 10.8 GHz–11.44 GHz with absorption bandwidths of 0.2 GHz, 0.2 GHz, and 0.64 GHz, respectively. It is crucial to mention that the bandwidths of the two last absorption peaks, 10.98 GHz and 11.29 GHz, are combined to achieve an enhanced bandwidth of 0.64 GHz. The proposed multi-band MTMA could be used in military applications, satellite communications and radar technology. Figure 2(b) describes the magnetic field distribution simulated by the CST program at four different peaks. At a resonance frequency of 5.6 GHz (peak 1) the magnetic field distribution is located only on the L-shaped part of the resonator, but when the frequency is increased to 7.6 GHz (peak 2) the magnetic field is strongly located at the square-shaped resonator. At a third peak (10.98 GHz resonance frequency), the magnetic field is located at both L- and square-shaped resonators, while at 11.29 GHz the magnetic field is weakly concentrated on the square resonator (peak 4).

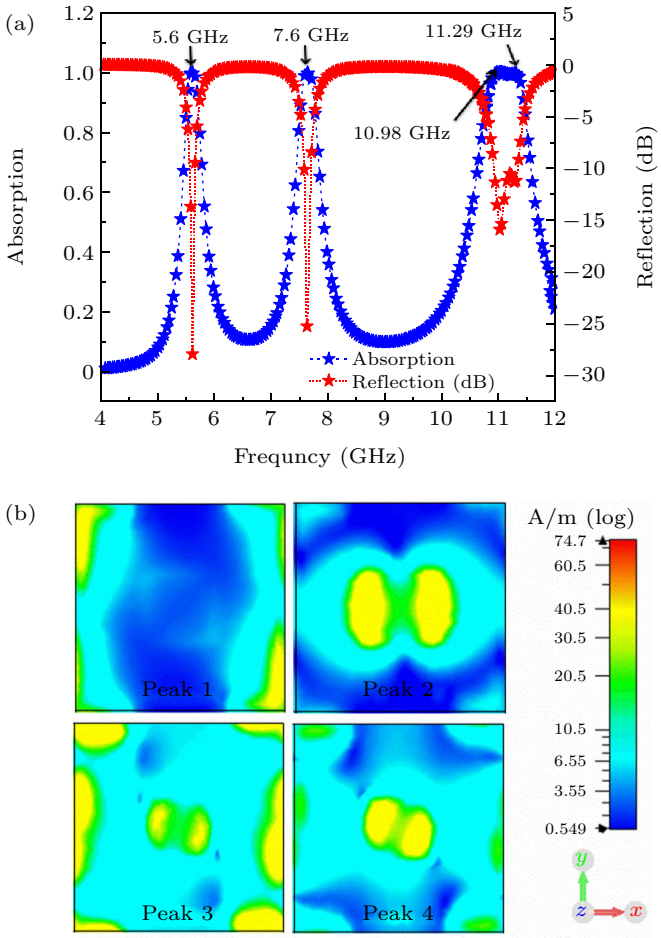


Fig. 2. (a) Simulated absorption and reflection of the multi-band MTMA. (b) Magnetic field distribution at four different peaks.

In this work, the proposed multi-band MTMA consists of the combination of two basic designs, namely design 1 and design 2, as shown in Figs. 3(a) and 3(b), respectively. In design 1, two symmetric L-shaped resonators were used in different orientations. The L-shaped resonators produce a resonance frequency at 5.6 GHz. However, the vertical sides also generate further modes which resonate around 11.3 GHz with a low absorption value. Design 1 consists of the two L-shaped resonators deposited on a FR4 dielectric layer with a thickness of 1.6 mm. The backside of design 1 is covered by copper metal with a thickness of 0.035 mm and a conductivity σ of 5.8×10^7 S/m. The FR4 substrate has a relative permittivity of 4.4 and a loss tangent ($\tan\delta$) of 0.02. The parameters

and the position of the resonators operate in the C and X frequency ranges. We used a genetic algorithm to optimize design 1. The dimensions of design 1 are shown in Table 1. As discussed before, the reflection values of the structure determined by the simulation software were used in Eq. (4) to get the absorption curve illustrated in Fig. 3(d). It can be seen from the red curve that there are two peaks at 5.63 GHz and 11.033 GHz corresponding to absorption of 99% and 84%, respectively. Moreover, design 2 consists of two resonators — a closed circular ring (CCR) resonator and a closed square ring (CRR) resonator. These two resonators are the basic types of microstrip resonator, and their resonance frequencies can be easily controlled through the resonator dimensions such as radius and line width. Therefore, each of these resonators can be operated at any desired frequency. Design 2 comprises a ring resonator inside the quadratic shape on the top of the FR4 substrate, while the bottom layer remains as in design 1. The absorption curve of design 2 is shown by the green curve in Fig. 3(d): note that the absorptivity of this design is greater than that of design 1 due to the resonator shape and coupling effect between the two resonators and the dielectric layer. The absorption is over 90% at 7.72 GHz and 11.55 GHz. Figure 3 shows a comparison of structure and absorption for these two designs with those of the proposed one. The blue curve in Fig. 3(d) has intensive multiple peaks at four different resonance frequencies which are compatible with the C and X frequency ranges. In our work, we tried to get the CRR to produce resonance at 7.6 GHz and the CRR to produce resonance at around 11.5 GHz. The design process includes different steps such as a parametric study and use of a genetic algorithm to understand the behavior of all resonators. Later, when designs 1 and 2 were combined, the two resonance frequencies around 11.3 GHz and 11.5 GHz combined, providing a wider bandwidth of 0.64 GHz due to a mutual coupling effect between the CCR and L-shaped resonators. Furthermore, there is a strong relation between the two resonance frequencies of 10.98 GHz and 11.29 GHz. It can be said that the vertical sides of the L-shaped resonator participated in producing the resonance frequency of 11.29 GHz as shown in Fig. 5(d). Because of this coupling effect, absorption of the lower resonance frequency improved and the higher resonance shifted to the left compared with the individual reflection results for designs 1 and 2. Therefore, the positions and dimensions of both the L-shaped resonator and the closed ring resonator were carefully optimized to yield the improved bandwidth of 0.64 GHz (10.8 GHz–11.44 GHz).

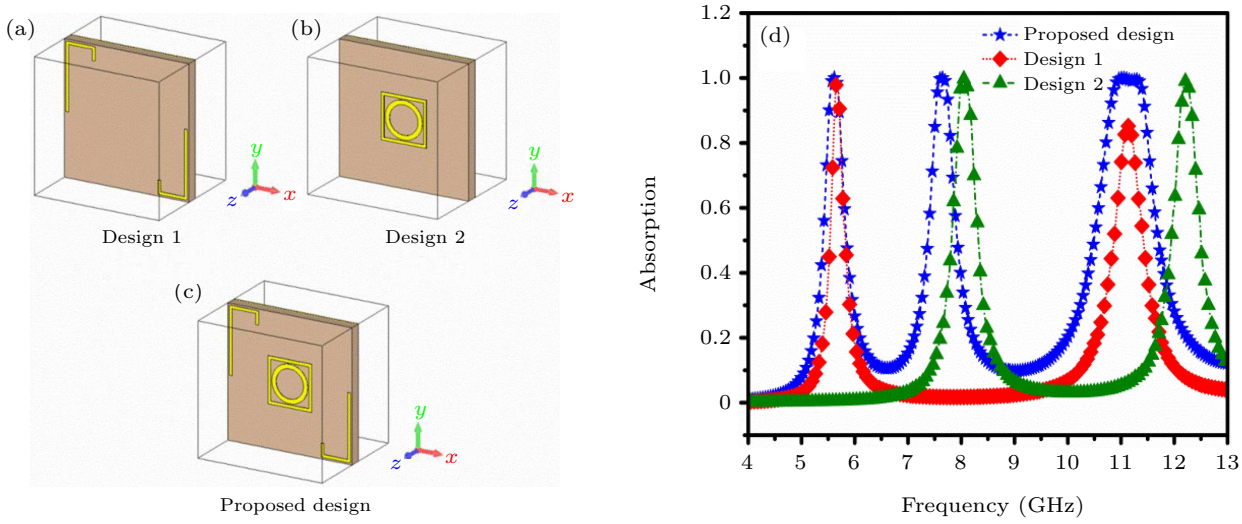


Fig. 3. Comparison of the three different designs: (a) design 1, (b) design 2, (c) proposed design. (d) Simulated absorption results.

In this work, the effect of changing the source polarization and incident angle on the designed MTMAs was monitored (see Fig. 4). It was assumed that the absorber was located in the XY plane. The incident angle is represented by θ (the angle in the ZX or ZY plane). Therefore, an absorber is said to be insensitive for changing incident angle when the absorption value is not changed by variation in the value of θ. Polarization is represented by φ (the angle in the XY plane). Therefore, an absorber is said to be insensitive for polarization angle when the absorption value is not changed by variation in the value of φ. To test the polarization sensitivity of the designed absorber, the direction of the propagating electromagnetic wave was fixed at normal incidence while the directions of electric and magnetic fields were changed at different polarization angles φ from 0° to 60° in steps of 15°.

As is clear from Fig. 4(a), at the lower frequency range the curves of the first and second peaks are almost the same but in the higher frequency range there is a shift in the two resonance frequencies of 10.98 GHz and 11.29 GHz while the absorption spectrum remains almost the same with changing polarization angle over the entire frequency range. Therefore, it is concluded that the proposed MTMAs are independent of

the polarization of the electromagnetic waves.

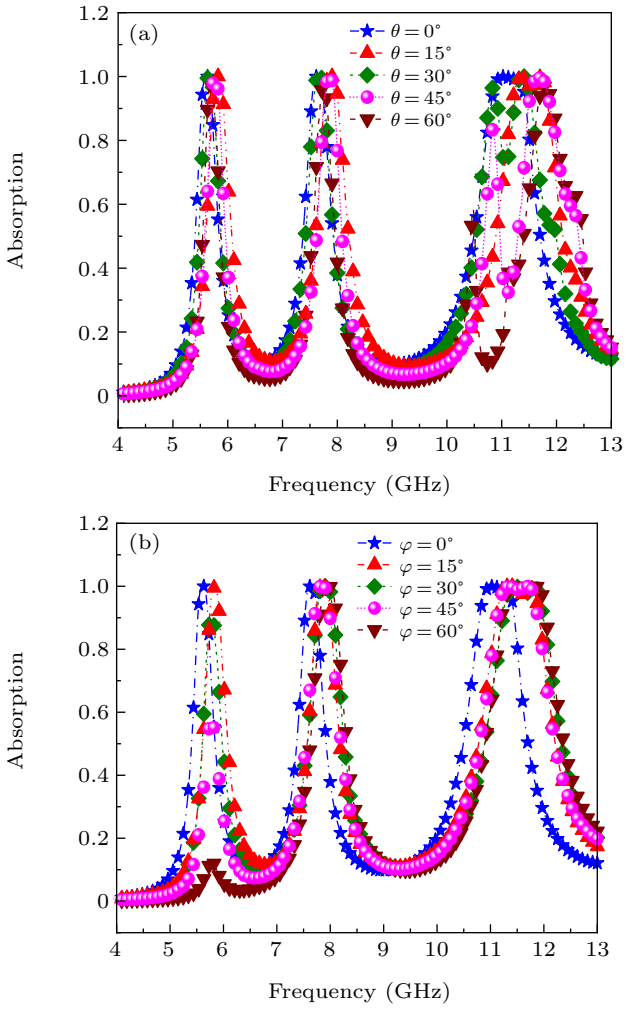


Fig. 4. Simulated absorption results at different (a) incident angles (θ) and (b) polarization angles (φ) for the multi-band metamaterials absorber.

In Fig. 4(b), we numerically investigate the absorption under an oblique incident angle because in some practical applications the electromagnetic waves are usually incident with an oblique angle. In this case, the angle θ is changed from 0° to 60° in steps of 15° and the other parameters remain constant during the simulation process. As can be seen from the curve, when the polarization angle is changed the absorption of the proposed structure remains higher than 90% in the frequency range from 2 GHz–13 GHz. Only in the higher frequency range is a small shift in the resonance frequency observed. It can be concluded from these two curves that the proposed structure is independent of the polarization angle and has sensitivity properties.

Figure 5 shows the simulated surface current distribution of a single unit cell of a MTMA. It is observed that each resonator of the MTMA structure is responsible for producing each resonance frequency in the band of interest. The concentration of surface current is found on the right and left of the L-shaped resonator and corresponds to the resonance frequency of 5.6 GHz in Fig. 5(a). Similarly, a concentration of surface current is found at the vertical sides of the square closed ring and corresponds to a resonance frequency of 7.6 GHz in Fig. 5(b). The current distribution can be seen along the vertical sides of L-shaped resonators at reduced concentration; this is responsible for producing the third resonance frequency of 10.98 GHz. Moreover, the current distribution at the last resonance frequency of 11.29 GHz is gathered along the circular ring resonator and horizontal line of the L-shaped resonator with high strength.

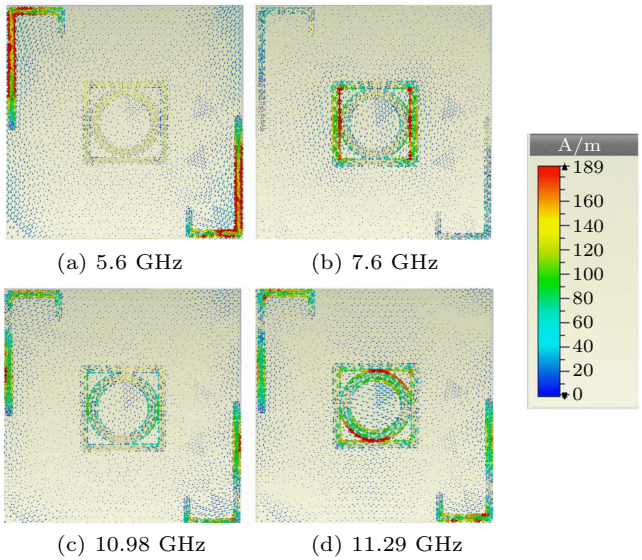


Fig. 5. Simulated surface current distribution of the proposed MTMA at the four absorption peak frequencies of (a) 5.6 GHz, (b) 7.6 GHz, (c) 10.98 GHz and (d) 11.29 GHz

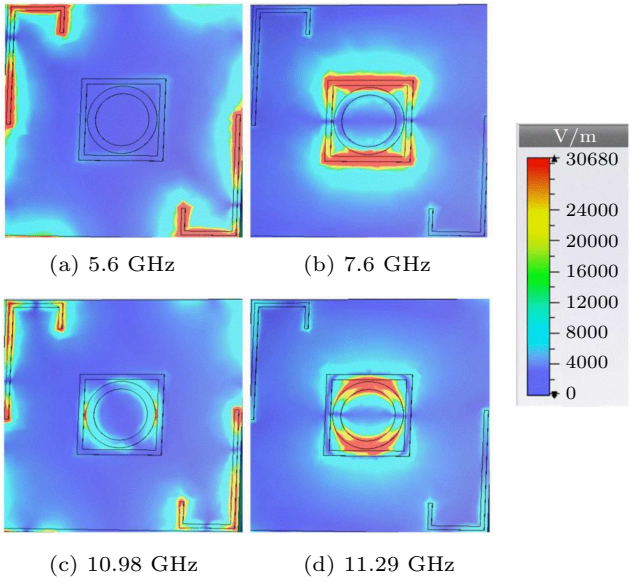


Fig. 6. Simulated electric field distribution at the four different resonance peaks.

Figure 6 shows the simulated electric field distributions on the XY plane of single-unit cells at resonance frequencies of 5.6 GHz, 7.6 GHz, 10.98 GHz, and 11.29 GHz under normal incidence ($\theta = 0°$). Similar to the current distribution, the strength of the electric field distribution can be seen on each

resonator structure at the corresponding resonance frequency. The electric field distributions at 5.6 GHz and 10.98 GHz are due to the effect of the L-shaped resonator. The frequency of 7.6 GHz is strongly affected by the vertical sides of the square closed ring. Moreover, the final resonance frequency of 11.29 GHz is due to the closed circular ring resonator. Further explanations can be given related to the shape of the resonators with current and electric field distributions. Because of the asymmetry of the L-shaped resonators, when the structure rotates with different angles φ, the positions (arrangement) of the L-shaped resonators change, causing a reduction of the current and electric field. Therefore, the L-shaped resonators are no longer responsible for producing resonance behavior at 5.6 GHz, especially in the worst case at 60°.

3. Absorption performance

For further verification, the electrical properties (permittivity, permeability, reflective index and impedance) of the proposed multi-band absorber are extracted in this section. The retrieval method is used for the extraction, which is based on the scattering parameters reflection coefficient S_{11} and the transmission coefficient S_{21}. To obtain these four parameters in simulation, the Nicolson–Ross–Weir method was used by taking the phase and magnitude of parameters S_{11} and S_{12} obtained in CST simulations. As can be seen from Figs. 7(a) and 7(b), the permittivity and permeability parameters have very similar dispersion to each other at resonance frequencies and the real parts of them are negative. Note that the proposed design has negative characteristics. Figure 7(c) depicts the real and imaginary parts of the refractive index for the proposed design; it can be seen from the curve that the imaginary part of the refractive index is negative at resonance frequencies. Figure 7(d) shows the normalized impedance of the multi-band MTMA. The real part of the normalized impedance is close to one and the imaginary parts are close to zero at resonance frequencies, indicating that the impedance of the proposed multi-band MTMA is matched with the free space impedance. The values of the real and imaginary parts of the designed absorber at resonance frequencies are shown in Table 2.

Table 2. Real and imaginary parts of the proposed MTMA at resonance peaks.

Frequency (GHz)	5.6	7.6	10.98	11.29
Real part impedance (Z)	1	3	1.1	2.3
Imaginary part impedance (Z)	0	0	0	0

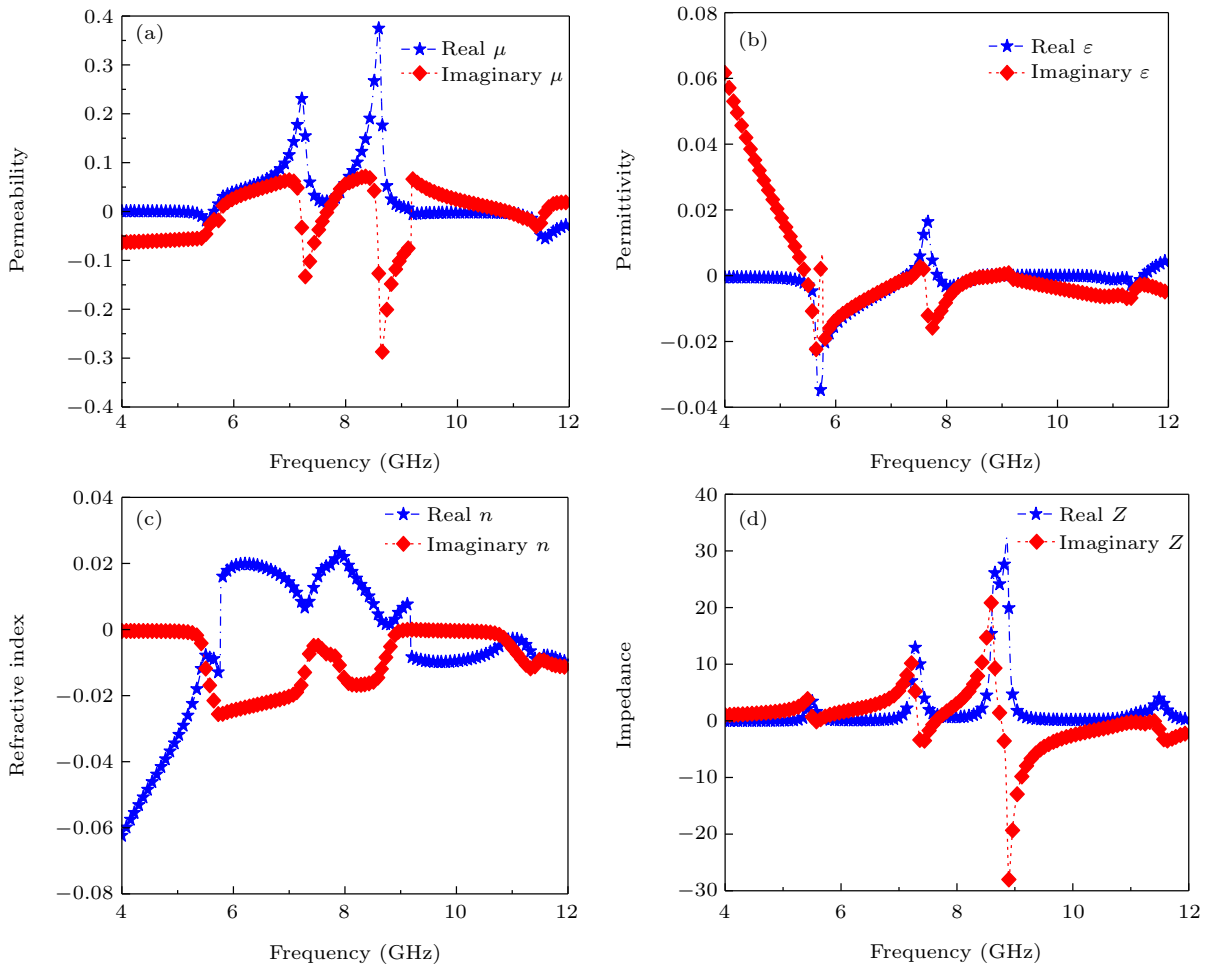


Fig. 7. Absorption performance: (a) permeability, (b) permittivity, (c) refractive index, and (d) impedance for proposed multi-band metamaterial absorber.

4. Fabrication of the proposed structure and comparison between simulated and experimental results

Two methods can be used for measuring the designed absorbers in the laboratory. In the first method a single cell of fabricated absorber is placed between two waveguide structures that are connected to either port of a VNA. In this method, the absorber should be of such as size that it fits into the aperture of the waveguide. Therefore, the dimensions of the absorber during the design process should be carefully optimized to obtain good results. In this work, we used the second method based on a horn antenna. The fabricated absorber can be put in front of a horn antenna that is connected to one of the VNA ports. In this method, the size of the fabricated absorber sheet should be taken into consideration. The larger manufactured structure leads to more accurate measurement results. Figure 8(a) shows the 7×5 unit cells of the designed absorber fabricated using a LPKF E-33 CNC circuit printer machine as shown in Fig. 8(b). The measurement setup for measuring the reflectivity of the fabricated absorber structure was prepared as shown in Fig. 9. The manufactured absorber was placed on the sample in front of the broadband (3 GHz–18 GHz) horn antenna. The measurement was repeated for different distances between the absorber structure and the antenna to achieve more accurate results. In the optimal case, the distance was set to be 15 cm and the far-field condition was confirmed.

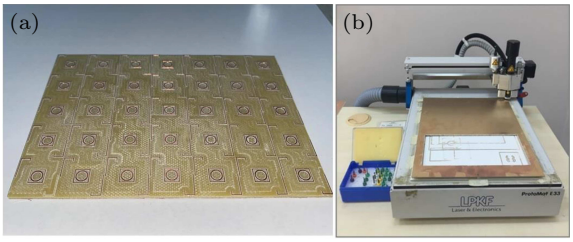


Fig. 8. Manufactured multi-band MTMA: (a) 7×5 unit cells and (b) fabricated design using a CNC based printed circuit board prototyping machine.

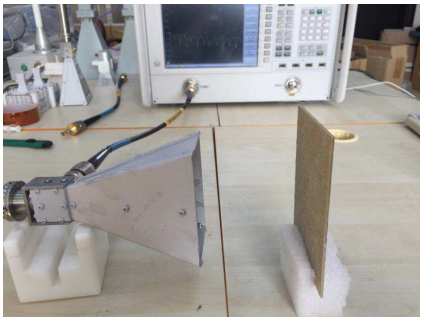


Fig. 9. Experimental measurement setup of the proposed multi-band MTMA using a horn antenna connected to a VNA.

A comparison of the obtained measurements with the simulation results is presented in Fig. 10. It can be seen from Fig. 10(a) that the measured values of the reflection coefficient are well matched with the simulation results. The measured results show resonance frequencies at 5.98 GHz, 7.7 GHz, and 11.15 GHz with −16.4 dB, −42 dB, and −24 dB, respectively. The corresponding absorption response of the absorber is shown in Fig. 10(b). As in the simulation results, almost perfect absorption can be achieved at all bands, whereas a small frequency shift is observed at the first band toward the higher frequency range.

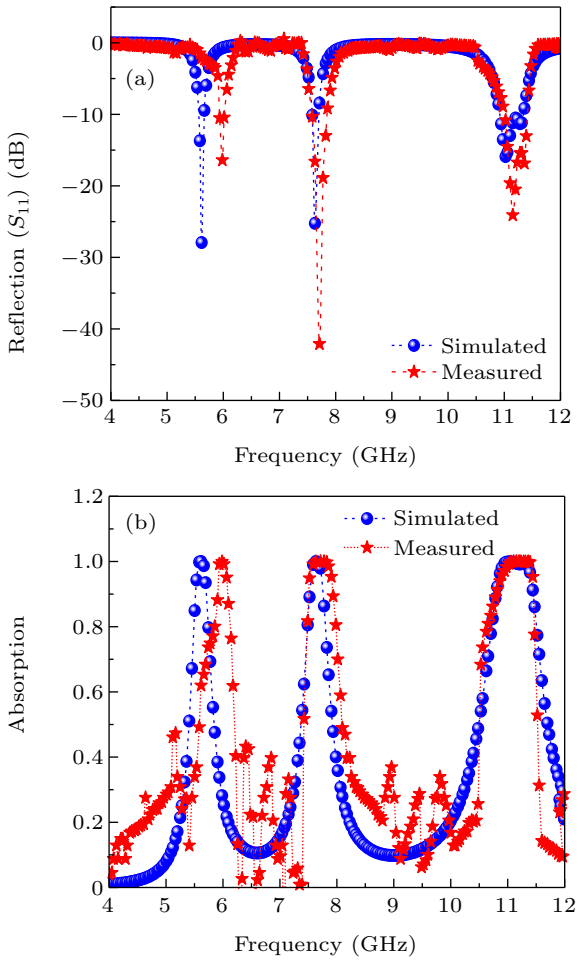


Fig. 10. Comparison of simulated and measured results: (a) reflection coefficient, (b) absorption for the multi-band MTMA using the horn antenna method.

It is clear from Fig. 10 that the results measured using the horn antenna are in good agreement with the simulation results. The measured results are a bit different from the simulated ones due to the manufacturing process and calibration errors in the VNA connecting the coaxial cables. The results obtained in this work are compared with those of other similar published papers in Table 3. Comparisons are given for unit cell dimensions, frequency band, dielectric substrate, maximum absorption rate, number of bands, resonance frequency and bandwidth. It can be seen from Table 3 that the proposed structure is of a smaller size than in other previously reported works; it can be used for dual-band applications, has four resonance frequencies and has the largest absorption bandwidth.

Table 3. Comparison of the results of the current work with other reported works in literature.

Ref.	Unit cell dimensions (mm^2)	Frequency bands	Substrate	Max. absorption rate (%)	No. of bands	Resonance frequency (GHz)	Absorption bandwidth (GHz)
[3]	35×35	C band	Arlon DiClad 527	98, 95	two	6.46, 7.68	0.12 (6.4–6.52)
[25]	20×20	C band	FR4	97, 99	two	5.6, 6	0.4 (5.8–6.2)
[26]	18×18	L, S and C bands	FR4	99	one	5.2	0.5 (5–5.5)
[27]	8×8	X and Ku bands	FR4	100	one	16	0.7 (15.7–16.4)
[28]	28.2×28.2	C band	FR4	91, 98.9, 99.5	three	4.2, 7, 7.4	0.4 (4–4.4)
[29]	30×30	C and X bands	FR4	99.87, 99.98, 99. 99	three	6.16, 8.76, 12.54	0.45 (5.8–6.25)
This work	18×18	C and X bands	FR4	100,100, 99, 99	four	5.6, 7.6, 10.98, 11.29	0.64 (10.8–11.44)

5. Conclusion

In summary, a new design for a multi-band metamaterial absorber has been investigated both numerically and experimentally for C and X band applications. According to the obtained results, four high-absorption peaks (100%, 100%, 99%, and 99%) are observed at 5.6 GHz, 7.6 GHz, 10.98 GHz, and 11.29 GHz, respectively. Negative parameters such as permeability, permittivity, refractive index and impedance have been extracted for the desired frequency range of 4 GHz–12 GHz. Our design is polarization-independent when the angle changes from 0° to 60°. The proposed structure has been manufactured and tested with a horn antenna and the numerical and experimental results are in good agreement. The surface current and electric field distributions have been studied. The multi-band metamaterial absorber can be used in many applications such as radar applications.

Acknowledgments

The authors would like to thank the Department of Electrical and Electronics, Iskenderun Technical University, Hatay, Turkey, for fabricating the designed structure. Also, we would like to thank the Department of Electrical Engineering and the Department of Telecommunication Engineering, Faculty of Engineering, Rajamangala University of Technology Rattanakosin, Thailand, for fabricating and measuring the single-designed structure.

References

[1] Altıntaş O, Aksoy M, Ünal E, Karaaslan M and Sabah C 2020 *Journal of the Electrochemical Society* **167** 147512
[2] Abdulkarim Y I, Deng L, Luo H, Huang S, Karaaslan M, Altıntaş O and Al-badri K S L 2020 *Journal of Materials Research and Technology* **9** 10291
[3] Bakıra M, Karaaslanb M, Unalb E, Akgolb O and Sabah C 2017 *Opto-Electronics Review* **25** 318
[4] Altıntaş O, Aksoy M and Ünal E 2020 *Physica E* **116** 113734
[5] Alkurt F O, Altintas O, Bakir M, Tamer A, Karadag F, Bagmanci M and Akgol O 2018 *Materials Science* **24** 253
[6] Alkurt F O, Altintas O, Ozakturk M, Karaaslan M, Akgol O, Unal E and Sabah C 2020 *Phys. Lett. A* **384** 126041
[7] Duan X, Chen X, Zhou Y, Zhou L and Hao S 2018 *IEEE Antennas and Wireless Propagation Letters* **17** 1617
[8] Aziz C H and Al-Hindawi A M 2016 *Journal of Modeling and Simulation of Antennas and Propagation* **2** 13
[9] Singh A K, Abegaonkar M P and Koul S K 2017 *IEEE Antennas and Wireless Propagation Letters* **16** 2388
[10] Farahani M, Pourahmadazar J, Akbari M, Nedil M, Sebak A R and Denidni T A 2017 *IEEE Antennas and Wireless Propagation Letters* **16** 2324
[11] Fang Z, Li J and Wang X 2020 *Computers & Mathematics with Applications* **79** 1165
[12] Manjappa M, Pitchappa P, Wang N, Lee C and Singh R 2018 *Advanced Optical Materials* **6** 1800141
[13] Zhang F, Li C, Fan Y, Yang R, Shen N H, Fu Q and Soukoulis C M 2019 *Advanced Materials* **31** 1903206
[14] Roosta Z, Keshavarz A and Honarasa G 2018 *Optik* **174** 648
[15] Chen H, Chan C T and Sheng P 2010 *Nat. Mater.* **9** 387
[16] Rosenblatt G and Orenstein M 2015 *Phys. Rev. Lett.* **115** 195504
[17] Alkurt F Ö, Altıntaş O, Bakır M, Karaaslan M, Ünal E, Karadag F and Sabah C 2020 *Optical Engineering* **59** 087104
[18] Bilal R M H, Baqir M A, Choudhury P K, Karaaslan M, Ali M M, Altıntas O and Sabah C 2021 *IEEE Access* **9** 5670
[19] Abdulkarim Y I, Deng L, Luo H, Huang S, He L, Yuhan L and Karaaslan M 2020 *Bull Mater. Sci.* **43** 116
[20] Han X, Zhang Z and Qu X 2020 *Optik* **228** 166086
[21] Mahmud S, Islam S S, Mat K, Chowdhury M E, Rmili H and Islam M T 2020 *Results in Physics* **18** 103259
[22] Zamzam P, Rezaei P and Khatami S A 2021 *Physica E* **128** 114621
[23] Yueyi Y, Kuang Z, Kuang Z, Xumin D, Badreddine R, Shah N B and Qun W 2019 *Photonics Research* **7** 80
[24] Yadgar I, Abdulkarim A, Fatih O, Alkurt C, Halgurd N, Awl D, Fahmi F, Muhammadsharif E, Mehmet B, Sekip D G, Muharrem K C and Heng L B 2021 *Result in Physics* **26** 104644
[25] Saeid Jamilan, Mohammad N A and Davoud Z 2014 *Progress In Electromagnetics Research C* **47** 95
[26] Majid A, Farzad T, Negin S, Justin L and Mehran A 2020 *Scientific Reports* **10** 13638
[27] Thi H N, Son T B, Trong T N, Thanh T N, YoungPak L, Manh A N and Dinh L V 2014 *Advances Natural Science: Nanoscience Nanotechnology* **5** 025013
[28] Sreenath R T, Naveen M and Raghvendra K C 2017 *AEU-International Journal of Electronics and Communications* **82** 508
[29] Ben M, Shaobin L, Borui B, Xiangkun K, Haifeng Z, Zhiwen M and Beiyin W 2014 *Journal of Electromagnetic Waves and Aplications* **2** 1
[30] Yueyi Y, Kuang Z, Badreddine R, Qinghua S, Xumin D, Qun W, Shah N B and Patrice G 2020 *Nat. Commun.* **11** 4186
[31] Kuang Z, Yueyi Y, Xumin D, Haoyu L, Badreddine R, Qun W, Jian Shah Nawaz B, Jiubin T 2021 *Laser & Photonics Reviews Applications* **1** 2000351
[32] Hema O A and Al-Hindawi A M 2021 *Journal of Engineering* **27** 1